2 Gas Fluidized Bed Polymerization

Argimiro R. Secchi
Gustavo A. Neumann
Rossano Gambetta

CONTENTS

2.1 Introduction

The petrochemical polymer industry is one of the most competitive around the world, dealing with commodities production, then for its survival, there is a constant need for production cost reduction, product quality gain, and research of new products. These needs brought investment in research, which fructified as process and product knowledge that allowed the development of representative process models and its application in process control (Embiruçu et al. 1996), e.g. predictive control and virtual analyzers, process engineering (Meier et al. 2002), e.g. new catalyst development, plant scale-up and design, and product development, e.g. time and cost reduction to development of new products by using computer based simulations. Therefore, obtaining a tool for process and control studies is the main motivation for the development of dynamic models for fluidized-bed polymerization reactors.

The first work on modeling a gas-phase polymerization reactor is due to Choi and Ray (1985), which had the objective of understanding the reactor dynamic behavior. Their model included the mass and heat transfer effects of the fluidized bed and a basic kinetic scheme. After their work, other authors as Lagemann (1989) and McAuley (1991) proposed more comprehensive models and some simplifications that could be used without losing much phenomenological information.

Meier et al. (2002) studied the temperature profile caused by catalyst segregation in a small-scale Fluidized-Bed Reactor (FBR) under semi-batch propylene polymerization. Their objective was controlling the particle size segregation in a laboratory scale to attain profiles similar to those found in industrial units. A model capable of predicting temperature profile and molecular weight distribution was developed as a tool to help the problem analysis. The proposed model uses multiple compartment approach, segmenting the reactor in a cone region, the draft tube, and the annulus, all of them considerate as a Continuous Stirred Tank Reactor (CSTR). The model uses some considerations normally found in the literature for this kind of reactor. The authors claimed that none of the previous published models were confronted with experimental data. However, the work of Gambetta (2001) and Gambetta et al. (2001) used experimental data to validate the proposed models, showing that a simpler model can be used to represent the real system with respect to production and some properties as Melt Index (MI) and density.

Fernandez and Lona (2001) assumed a heterogeneous three-phase model (i.e., gas, emulsion and solid phases) where plug flow was assumed for all phases, and the reactions take place only in the emulsion phase due to the common assumption that the bubbles are solid-free. Later, these authors presented a model for multizone circulating reactor for gas-phase polymerization, which consists of two interrelated zones with distinct fluid dynamic regimes where the polymer particles are kept in continuous circulation (Fernandez and Lona 2004).

Kiashemshaki et al. (2004) used the model by Meier et al. (2002) for the polyethylene polymerization with Ziegler-Natta catalyst system. The authors included some correlations capable to predict MI and density of the produced polymer from its mass average molecular weight ($\bar{M}_w$) and confronted their simulated results with actual industrial plant data. Alizadeh et al. (2004) used a tank-in-series model approach to model a polyethylene producing reactor that uses a Ziegler-Natta catalyst system (using a two catalyst site kinetic scheme), to attain a behavior between a plug-flow reactor and a CSTR. Each CSTR was modeled as two-phase flow structure to better represent the fluidized bed. The authors compared model predictions with

experimental MI, and presented dynamic responses of the predicted production and some molecular weight distribution parameters (mean molecular weights and polydispersity index) without respective experimental results.

Later, Kiashemshaki et al. (2006) created a FBR model for polyethylene production using the dynamic two-phase concept associated with Jafari et al. (2004) hydrodynamic model. The fluidized bed was segmented in four sections in series, where the gas phase and emulsion phase were considered plug flow reactor and perfected mixed reactor, respectively, each one of them exchanging heat and mass with its counterpart. The gas flow goes upward from the bottom and the particles goes downward, with the polymer leaving the system from the bottom. The gas phase was modeled with catalyst particles, producing polymer as well the emulsion phase. The authors found that 20% of the polymer is produced in the gas phase. The model predicts monomer concentration profiles, polymer productivity, reactor temperature, and produced polymer molar mass distribution and polydispersity index, and all predictions have been compared with industrial experimental data.

Ibrehema et al. (2009) implemented a model for gas-phase catalyzed olefin polymerization FBR using Ziegler–Natta catalyst. On their approach four phases were used: bubbles, cloud, emulsion, and solids, each one with its respective mass and heat transfer equations, and reactions occurring at the catalyst surface (solid phase) present inside the emulsion phase. Catalyst type and particle porosity were included in the model, having effect over reaction rates. The authors studied the temperature and concentration profiles in the bubble and emulsions phases, the effect of catalyst on the system, as well the superficial gas velocity, catalyst injection rate, and catalyst particle growth on the FBR dynamic behavior, comparing the results with those of other developed models (i.e., constant bubble size, well-mixed and bubble growth models). Steady-state simulation results of molar mass distribution and polydispersity index of the produced polymer were also compared with experimental data.

More recently, there are some researches about Computational Fluid Dynamics (CFD) simulation of individual particles and their interactions in FBR for polyolefin production. A review on these CFD models applied to FBR was published by Mahecha-Botero et al. (2009). Eulerian–Eulerian two-fluid model that incorporates the kinetic theory of granular flow was used in most of the works to describe the gas-solid two-phase flow in the fluidized bed polymerization reactors (Dehnavi et al. 2010, Rokkam et al. 2011, Chen et al. 2011a, 2011b). CFD is an emerging technique to study FBR and holds great potential in providing detailed information on its complex fluid dynamics. However, these studies still lacks of substantial experimental validation.

In this chapter, two dynamic models are presented for the copolymerization of ethylene in a FBR: a phenomenological model traditionally used for control and process engineering applications, and a reduced model used as a tool for estimation of kinetic parameters. The main relevance of this work is the methodology that takes a model developed for use in control and process studies, and replaces some of its states by their correspondent plant measurements. As shown in the results, the application of this methodology does not imply in any loss of information, in terms of production and final polymer properties. Combinations of the obtained phenomenological model with empirical models are also discussed as applications for process monitoring and control.

2.2 Process Description

The main characteristic of the gas-phase polymerization processes is the absence of a liquid phase in the polymerization zone, with the reaction occurring at the interface between the solid catalyst and the gas adsorbed by the amorphous phase of the polymer. The gas phase maintains the reaction by providing the monomer, mixing the particles, and removing heat from the system.

The first gas-phase polymerization process of olefins was the BASF process in the 60's, operating at 30 bar and 100°C. In the same period, NOVOLEN® (BASF Akfiengesellschaft, Ludwisghafen, DE) process was developed using a similar stirred bed reactor in gas phase, operating below 20 bar and temperatures from 70 to 92°C, and using a helical stirrer instead of an anchor stirred used in the former process to maintain uniform the reacting conditions (Reginato 2001). The unreacted monomer was condensed and recycled to remove the heat of reaction. Due to mechanical agitation instead of fluidization, the monomer recirculation had to be minimized. Currently, the most widely used process for producing olefin in gas phase is the UNIPOL™ (The Dow Chemical Company and affiliated, Midland, Michigan) process, described in the following section.

McAuley et al. (1994a), Zacca (1995) and Peacock (2000) conducted a review on the existing gas-phase polymerization processes, the employed catalyst and involved reactions, and the polymer properties and characterization.

2.2.1 UNIPOL Process

As can be seen in the simplified schema of the UNIPOL process, showed in Figure 2.1, the reactor is composed by a fluidized-bed zone, where the reactions occur, and a disengagement zone, responsible for removing the light particles before they can enter the recycle. A heat exchanger is used to remove the reaction heat from the recycle stream, and then the cooled gas is compressed and mixed with the gaseous feed stream and re-injected at the base of the reactor. The solid catalyst is fed in a stream of fresh nitrogen by the feeder, and then dragged to the fluidized bed. The product is removed from the fluidized-bed zone by a system of discharge vases, which operates in cycles determined by the production rate of the reactor. In the disengagement zone the gas composition is analyzed by chromatography.

2.2.2 SPHERILENE Process

The SPHERILENE (TM, LyondellBasell Group Compagies, Carroliton, Texas) process technology was developed by LyondellBasell using two gas-phase reactors in series, for the production of a wide density range of polyethylene, with the addition of co-monomers. Heterogeneous Ziegler-Natta catalyst is fed into a pre-contact vessel, where the catalyst is activated. The activated catalyst is fed into two pre-polymerization loop reactors in series before entering the FBRs. In these loop reactors, the catalyst is encapsulated with polypropylene to guarantee reaction controlled conditions in the FBRs. The FBR feed is formed by the activated

catalyst system and a mixture of ethylene, co-monomer, hydrogen and solvent, showed in Figure 2.2.
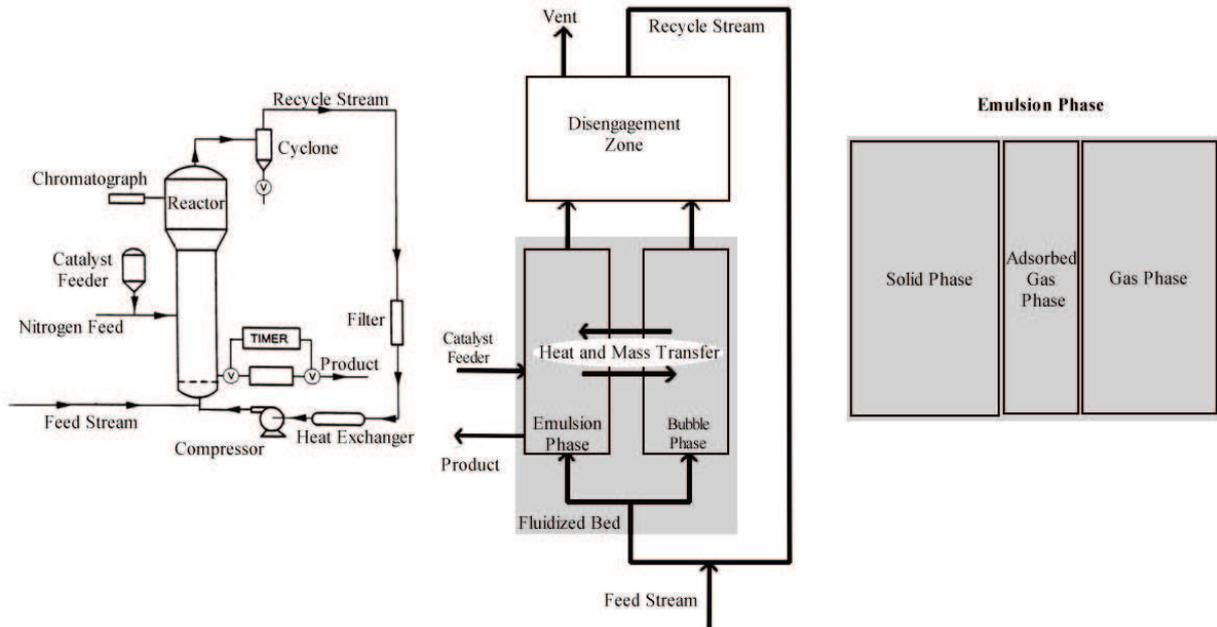
FIGURE 2.1 UNIPOL process (McAuley et al. 1994a) and reactor model zones.

A heat exchanger in each FBR is responsible to remove the polymerization heat. Product is continuously discharged from the first FBR to a system to separate the polymer and the dragged gas, which is recycled in a distillation system (not shown in Figure 2.2) to recover heavy and light gases and return them to the reactor. Active catalyst from the first FBR is fed together with the product to the second FBR to continue the reaction at the same or new conditions, depending on the properties required to the polyethylene. The second FBR has independent supply of ethylene, co-monomer, hydrogen, and solvent. The spherical polymer, with particle size ranging from approximately 0.5 mm to 3 mm, is then discharged in a unit to recover the gas, neutralize any remaining catalyst activity and dry the polymer.
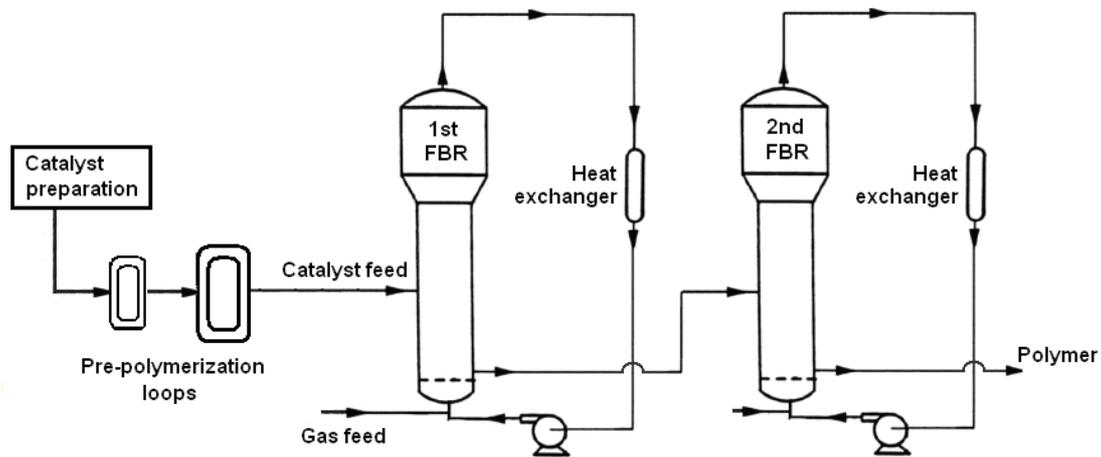
FIGURE 2.2 SPHERILENE process.

2.2.3 SPHERIPOL Process

The SPHERIPOL (TM, LyondellBasell Group Companies, Carroliton, Texas) process, developed by LyondellBasell, normally consists of two loop reactors in series to produce polypropylene. Some of these plants may have a fluidized-bed gas-phase reactor in series with the two loop reactors to incorporate a layer of copolymer of ethylene and propylene, as shown in Figure 2.3. Thus, it is possible to produce homopolymer polypropylene and many families of random and heterophasic copolymers.

After pre-contact and pre-polymerization, propylene, hydrogen and heterogeneous Ziegler-Natta catalyst system are fed into the two tubular loop reactors. The propylene in liquid phase acts as a solvent in a bulk polymerization in these reactors. In the production of materials highly resistant to impact, with high amounts of co-monomer, such as high-impact polymer (heterophasic copolymer), a FBR is used operating in series with loop reactors, which generates homopolymers. The non-reacted monomers are recycled to the reactor through a centrifugal compressor that keeps the fluidization of the bed with a feed stream of ethylene, hydrogen and propylene. Part of these monomers may also come from the stripping tower, which is part of the recovery section of the monomer unit. The hydrogen and propylene feeds are set according to gas chromatographic analysis of the feed stream and by the desired production of copolymer, which is specified by the desired hydrogen/ethylene and ethylene/(ethylene + propylene) molar relations in the reactor. The ethylene flow rate is defined as the percentage of ethylene that should be incorporated into the reactor.
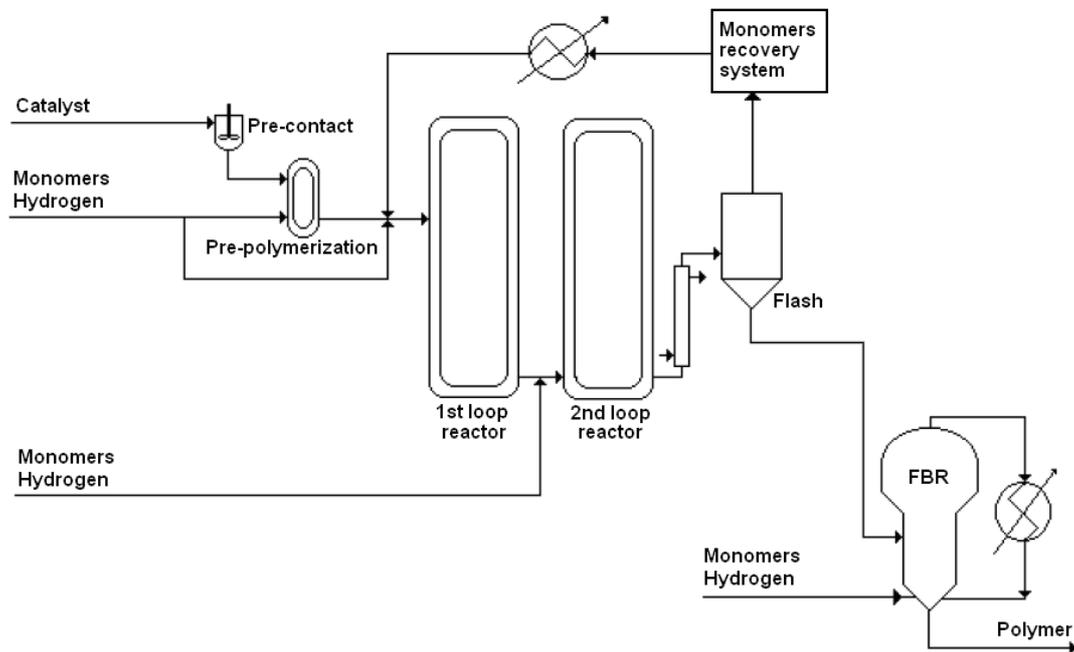
FIGURE 2.3   SPHERIPOL process.

2.3 Mathematical Modeling

The mathematical models presented in this section were developed for the fluidized-bed polymerization reactor of the UNIPOL process, using chromium-oxide catalyst system for the copolymerization of ethylene, propylene, and butene, producing high-density polyethylene and linear low-density polyethylene. However, this model can be extended to other catalyst systems (e.g. Ziegler-Natta), as well, FBRs of other processes, as SPHERILENE process (with two reactors in series) and some SPHERIPOL processes, that have a FBR in series with loop reactors.

A complete model was developed to be used in control and processes studies, while a reduced model was built for parameter estimation purpose. The most important process variables that characterize the product in this kind of reactors were the MI, density, and co-monomer fraction, all requiring lengthy off-line measurements, which justify the development of models to use in control applications (e.g. virtual analyzers). The following gaseous components have been considered in the model: ethylene, propylene, butene, hydrogen, nitrogen, oxygen, and impurities. All of them modeled as ideal gases.

2.3.1 Complete Model

The developed complete model was based on the works of Choi and Ray (1985), Lagemann (1989), McAuley (1991), and Secchi et al. (2001). In Figure 2.1, the FBR, with two distinct phases (bubbles and emulsion) that exchange heat and mass, has been modeled with the fluidization equations of Kunii and Levenspiel (1991), from which Choi and Ray (1985) defined a basic set of equations, and then this set was used and adapted by Lagemann (1989) and McAuley et al. (1994b). The set of equations used in this work is showed in Table 2.1.

The emulsion phase is composed by a solid phase (polymer, catalyst, and co-catalyst), a gas phase formed by the minimum flux of gas necessary to maintain the bed fluidized, and an adsorbed gas phase associated with the amorphous polymer. The gas in excess to the minimum fluidization condition constitutes the bubble phase, moving in plug-flow, and considered in quasi-steady state. The emulsion phase is considered homogeneous, and the product is removed with its composition.

Polymer crystallinity and swelling are assumed to be constant, and polymer density and MI are obtained from correlations (McAuley 1991, Kiashemshaki et al. 2004, Peacock 2000). The adsorbed gas phase in the amorphous polymer (in solid phase) is in equilibrium with the emulsion gas phase, and the reactions that occur in the solid phase are related to the adsorbed phase concentration.

This model uses as inputs the flow rates of each gaseous components, temperature and flow rate of the recycle gas, product removal, and gaseous vent. There are dynamic mass balances for all gaseous components in the gas phase (emulsion) and the disengagement zone, and there is one dynamic energy balance in each region. For the solid phase, there are mass balances for all types of sites and the low-order moments of the polymer. The moments are responsible for keeping track of the mean properties of the polymer per type of site and end group, including the average molecular weights, polydispersity index, number of active and dead polymer chains, and polymer composition.

TABLE 2.1
Equations used to model the fluidization

Description	Equation	Eq.	Reference
Void fraction at minimum fluidization conditions	$\varepsilon_{mf} = 0.586\left[\dfrac{\mu^2}{\rho_g\, g\left(\rho_s - \rho_g\right)d_p^3}\right]^{0.029}\left(\dfrac{\rho_g}{\rho_s}\right)^{0.021}$	(2.1)	Choi and Ray (1988)
Reynolds number at minimum fluidization conditions	$\mathrm{Re}_{mf} = \left(29.5^2 + 0.0357\,Ar\right)^{0.5} - 29.5$	(2.2)	McAuley et al. (1994b)
Arquimedes number	$Ar = \dfrac{d_p^3\,\rho_g\left(\rho_s - \rho_g\right)g}{\mu^2}$	(2.3)	
Superficial gas velocity at minimum fluidization conditions	$U_{mf} = \dfrac{\mathrm{Re}_{mf}\,\mu}{d_p\,\rho_g}$	(2.4)	Kunii and Levenspiel (1991)
Maximum bubble diameter	$d_{bm} = \dfrac{2U_T^2}{g}$	(2.5)	McAuley et al. (1994b)
Initial bubble diameter	$d_{bo} = 0.00376\left(U_0 - U_{mf}\right)^2$	(2.6)	Choi and Ray (1988)
Effective bubble diameter	$d_b = d_{bm} - \left(d_{bm} - d_{bo}\right)\exp\left(\dfrac{-0.3H}{2D}\right)$	(2.7)	
Terminal velocity of a falling particle	$U_T = \dfrac{4d_p\left(\rho_s - \rho_g\right)g}{3\rho_g\,C_D}$	(2.8)	Kunii and Levenspiel (1991)
Draft coefficient	$C_D = \dfrac{24}{Re_p} + 3.3643\,Re_p^{0.3471} + \dfrac{0.4607\,Re_p}{Re_p + 2682.5}$	(2.9)	
Particle Reynolds number	$\mathrm{Re}_p = \dfrac{d_p\,U_0\,\rho_g}{\mu}$	(2.10)	
Velocity of a bubble rising through a bed	$U_b = U_0 - U_{mf} + 0.711\left(g\,d_b\right)^{0.5}$	(2.11)	
Bubble fraction on emulsion phase	$\delta^* = \dfrac{U_0 - U_{mf}}{U_b}$	(2.12)	Choi and Ray (1988)
Upward superficial velocity of gas through the emulsion phase	$U_e = \dfrac{U_{mf}}{\varepsilon_{mf}\left(1 - \delta^*\right)}$	(2.13)	
Mass transfer between bubble and cloud-wake region	$K_{bc} = 4.5\dfrac{U_{mf}}{d_b} + 5.85\dfrac{D_g^{0.5}\,g^{0.25}}{d_b^{1.25}}$	(2.14)	
Mass transfer between cloud-wake region and emulsion phase	$K_{ce} = 6.78\left(\dfrac{\varepsilon_{mf}\,D_g\,U_b}{d_b^3}\right)^{0.5}$	(2.15)	
Mass transfer between bubble and emulsion phases	$K_{be} = \left(\dfrac{1}{K_{bc}} + \dfrac{1}{K_{ce}}\right)^{-1}$	(2.16)	Kunii and Levenspiel (1991)
Heat transfer between bubble and cloud-wake region	$H_{bc} = 4.5\dfrac{U_{mf}\,\rho_g\,c_{pg}}{d_b} - 5.85\left(\dfrac{\rho_g\,K_g\,c_{pg}}{d_b^{2.5}}\right)^{0.5}g^{0.25}$	(2.17)	
Heat transfer between cloud-wake region and emulsion phase	$H_{ce} = 6.78\left(\rho_g\,K_g\,c_{pg}\right)^{0.5}\left(\dfrac{\varepsilon_{mf}\,U_b}{d_b^3}\right)^{0.5}$	(2.18)	
Heat transfer between bubble and emulsion phases	$H_{be} = \left(\dfrac{1}{H_{bc}} + \dfrac{1}{H_{ce}}\right)^{-1}$	(2.19)	

The bubble phase is composed by the gas in excess to that necessary to maintain the emulsion at minimum fluidization conditions, modeled by steady-state mass and energy balances. The resulting equations that evaluate the average concentration for each component in the bubble phase, $\left[\bar{E}_{b,i}\right]$, are given by Equation 2.20. The concentration of each component of the gas going out from the bubble phase at the bed top, $\left[E_{b,i}^{k}\right]$, is given by Equation 2.21.

$$[\bar{E}_{b,i}] = [E_{g,i}] + \left([E_{0,i}] - [E_{g,i}]\right) \frac{U_b}{H.K_{be}} \left(1 - \exp\left(\frac{-H\,K_{be}}{U_b}\right)\right) \tag{2.20}$$

$$[E_{b,i}^{h}] = [E_{g,i}] + \left([E_{0,i}] - [E_{g,i}]\right) \exp\left(\frac{-H\,K_{be}}{U_b}\right) \tag{2.21}$$

In Equations 2.20 and 2.21, $\left[E_{g,i}\right]$ and $\left[E_{0,i}\right]$ represent the concentration of component i in the gas phase and the gas entering the bed from below, respectively; U_b represents the velocity of a bubble rising through a bed (Equation 2.11), H represents the height of the fluidized bed, and K_{be} represents the mass transfer coefficient between the bubble and gas phases (Equation 2.16).

The average temperature of the bubble phase, $\bar{T}_b$, is given by Equation 2.22. The temperature of the gas going out from the bubble phase at the bed top, T_b^{h}, is given by Equation 2.23.

$$\bar{T}_b = T + \left(T_o - T\right) \frac{U_b\,c_{Tb}\,c_{pg}\,\bar{M}_b}{H\,H_{be}} \left(1 - \exp\left(\frac{-H\,H_{be}}{U_b\,c_{Tb}\,c_{pg}\,\bar{M}_b}\right)\right) \tag{2.22}$$

$$T_b^{h} = T + \left(T_0 - T\right) \exp\left(\frac{-H\,H_{be}}{U_b\,c_{Tb}\,c_{pg}\,\bar{M}_b}\right) \tag{2.23}$$

In Equations 2.22 and 2.23, T is the temperature of the gas phase, T_0 is the temperature of the gas entering the fluidized bed from bellow, c_{Tb} is the total concentration of the bubble phase, c_{pg} is the specific heat of the gas phase, $\bar{M}_b$ is the mean molecular weight of the gas in the bubble phase, and H_{be} is the heat transfer coefficient between the bubble and gas phases (Equation 2.19).

The emulsion phase is composed by the solid phase (catalyst and polymer) and a gas phase, formed by the gas required to maintain the solid on minimum fluidization condition. The mass balances used to model this phase are represented by two equations, one for each gaseous component of the emulsion phase (Equation 2.24), and other for each solid component of the emulsion phase (potential, active and dead sites) and the polymer moments (Equation 2.25). The

polymer moments are used to maintain the registry of the main properties of the molecular weight distribution curve during a simulation.

$$\frac{dE_{g,i}}{dt} = U_e \, A \, \varepsilon_{mf} \left(1 - \delta^*\right)\left([E_{0,i}] - [E_{g,i}]\right)$$
$$+ K_{be}\left([\bar{E}_{b,i}] - [E_{g,i}]\right)V_b + F_{E_i,f} + R_{E_i}$$
$$- Q_p\left[\varepsilon_{mf}[E_{g,i}] + \left(1 - \varepsilon_{mf}\right)\left(1 - f_c\right)\chi[E_{gs,i}]\right]$$

(2.24)

$$\frac{dE_i}{dt} = F_{E_i,f} - Q_p\left(1 - \varepsilon_{mf}\right)\frac{E_i}{V_s} + R_{E_i}$$

(2.25)

In Equations 2.24 and 2.25, U_e is the gas velocity in the emulsion phase (Equation 2.13), A is the reactor area at the fluidized-bed region, ε_{mf} is the fluidized-bed porosity (Equation 2.1), δ^* is bubble fraction in the fluidized bed (Equation 2.1), V_b is the bubble-phase volume, $F_{E_i,f}$ is the molar flux of component i fed into the fluidized bed (e.g. a stream from another reactor), $R_{E,i}$ is the reaction rate (given in Table 2.4), Q_p is the volumetric flow rate of product, f_c is the crystallinity factor and χ is the swelling factor.

The energy balance for the emulsion phase is given by Equation 2.26.

$$\left(m_g . c_{pg} + m_s . c_{ps}\right)\frac{dT}{dt} = U_e \, A \, \varepsilon_{mf}\left(1 - \delta^*\right)\rho_{g0} \, c_{p0}\left(T_0 - T\right)$$
$$+ \sum_{i=1}^{nm}\left(-\Delta H_{R_i}\right)R_{M,i}\,\bar{M}_{M,i} - H_{be}V_b\left(T - \bar{T}_b\right)$$
$$+ K_{be}V_b\,c_{pb}\left(\bar{T}_b - T\right)\sum_{i=1}^{mc}\left(\left[\bar{E}_{b,i}\right] - \left[E_{g,i}\right]\right)\bar{M}_i$$

(2.26)

In Equation 2.26, m_g is the mass of gas in the emulsion phase, m_s is the mass of solids in the emulsion phase, c_{ps} is the specific heat of the solid phase, ρ_{g0} is the specific mass of the gas entering the fluidized bed from below, c_{p0} is the specific heat of the gas phase entering the fluidized bed, ΔH_{R_i} is the polymerization reaction heat, c_{pb} is the specific heat of the bubble phase, nm is the number of monomers, nc is the number of components, $\bar{M}_{M,i}$ is the molecular mass of the monomer i, $\bar{M}_i$ is the molecular mass of the component i, $R_{M,i}$ is the reaction rate of the monomer i.

The disengagement zone is responsible by the mixture of the gas streams that comes from the emulsion phase and the bubble phase, as well, a reservoir of gas, damping variations in the

gaseous feed of the system. This phase is modeled using a mass balance for each gaseous component (Equation 2.27) and an energy balance (Equation 2.28).

$$V_d \frac{d[E_{d,i}]}{dt} = U_e A \varepsilon_{mf} \left(1 - \delta^*\right)[E_{g,i}] + U_b A \delta^* [E_{b,i}^h] +$$
$$- \left(Q_v + Q_r\right)[E_{d,i}] - [E_{d,i}] \frac{dV_d}{dt} \qquad (2.27)$$

$$c_{pg} V_d \rho_d \frac{dT_d}{dt} = U_e A \varepsilon_{mf} \left(1 - \delta^*\right) \rho_e c_{p_g} \left(T - T_d\right)$$
$$+ U_b A \delta^* \rho_b c_{p_b} \left(\overline{T}_b - T_d\right) \qquad (2.28)$$

In these equation (Equations 2.27 and 2.28), $\left[E_{d,i} \right]$ is the concentration of the component i in the disengagement zone, Q_v is the vent volumetric flow rate, V_d is the volume of the disengagement, T_d is the disengagement zone temperature, ρ_d is the specific mass of the gas in the disengagement zone.

The global mass balance for the solid inside the reactor is defined in Equation 2.29, in which W_f is the mass flow rate of solid fed into the reactor. This equation is needed because all other phase volumes are defined as a function of the solid phase volume, obtained from mass of solid inside the reactor.

$$\frac{dm_s}{dt} = W_f - Q_p \left(1 - \varepsilon_{mf}\right) \rho_s - \sum_{i=1}^{nm} R_{M,i} \overline{M}_{M,i} \qquad (2.29)$$

The volume of the disengagement zone is that left out from the fluidized bed, and it changes as the mass of solid inside the reactor or the fluidization condition changes, as can be seen in Equation 2.30.

$$\frac{dV_d}{dt} = -\frac{1 - \chi \left(1 - \left(1 - \varepsilon_{mf}\right)\left(1 - \delta^*\right)\left(1 - f_c\right)\right)}{\rho_s \left(1 - \varepsilon_{mf}\right)\left(1 - \delta^*\right)\left(1 - \chi\right)} \frac{dm_s}{dt} \qquad (2.30)$$

The MI is one of the most important process variables in industrial plants, and is usually modeled by Equation 2.31 (McAuley 1991, Kiashemshaki et al. 2004, Alizadeh et al. 2004), in which a and b are model parameters, with values of 3.3543×10^{17} and -3.4722, respectively.

$$MI = a\,\overline{M}_w^{\,b} \tag{2.31}$$

2.3.2 Reduced Model

The necessity of closed-loop simulation to maintain the model in a certain operating condition as in the real plant was verified in the present model development. The attainable performance depends on the adjustment of the control parameters that are defined for a certain operating condition and group of kinetic parameters. It has been observed that the kinetic parameters that should be estimated are affected by the controller parameters. The problem consists, basically, in maintaining the model conditions that affect the reaction rates as close as possible to the operating conditions measured in the plant. This could be obtained by estimating the model parameters in closed loop. As a consequence, both, the kinetic parameters and the control parameters, need to be estimated. An alternative way would be to use more direct variables that are responsible for production and product properties.

The commercial software POLYSIM (Hyprotech Ltd., Calgary, Alberta associated with UWPREL, see: Ray 1997) adopted the use of a perfect control strategy, that is, to force the manipulated variable to assume the exact value to maintain the controlled variable in its set point. This strategy, however, has convergence problems for the simulation and, during the parameter estimation, could lead the manipulated variables to assume infeasible values.

The present work shows the possibility to use plant measurements that define the operating conditions of the reactor as inputs of a proposed reduced model for parameter estimation. The use of these variables as inputs results in the following advantages: 1) the operating conditions in the model are near those of the real plant, so when the kinetic parameters are well estimated, the outputs of the model should be close to the plant outputs, resulting in better convergence properties; 2) there is a considerable reduction in the number of differential equations, by reducing the number of mass and energy balances, resulting in a faster parameter estimation algorithm.

McAuley (1991) presented a dynamic kinetic model as an intermediary step to a full model used in control and process studies. This model has a structure similar to the model presented in this section, with the same inputs and capabilities to predict production and product properties. The kinetic parameters used by McAuley (1991), for Ziegler-Natta catalyst, were found in the literature, and some of them were manipulated to obtain a better fit between plant data and model prediction.

In the reduced model, some states measured in the plant are assumed to be inputs, as shown in Table 2.2. These inputs are the concentrations of the gaseous components, reactor temperature, mass of the fluidized bed, mass flow rate of catalyst and recycle gas flow rate. The recycle gas flow rate has been maintained for use with the fluidization equations, in order to calculate process variables as the bed height and the bulk density. As stated by McAuley et al. (1994b), the two-phase fluidized-bed model can be well described by a well-mixed reactor, so the reduced model uses only one well-mixed zone, with a gas phase and a solid phase.

This model reduction brought benefits such as a better convergence, and a smaller number of differential equations. In the simplest case, the complete model has 22 states while the reduced model has only 10. This is reflected on the computational time of the simulations: 70 hours of plant operation lasted 374 seconds of CPU for the complete model and 30 seconds of CPU of a Pentium IV/1.2GHz for the reduced model.

TABLE 2.2
Variables required at the construction of the models and the way that they are considerate in the models

Variable	Model	
	Complete	*Reduced*
Gaseous components concentrations	States (bed and disengagement)	Input (bed)
Gaseous components flow rates	Input or controlled	-
Catalyst Feed	Input	Input
Potential sites conc.	State	State
Active sites conc.	State	State
Dead sites conc.	State	State
Polymer moments	States	States
Bed temperature	States (bed and disengagement)	Input (bed)
Gas recycle temperature	Input or controlled	-
Bed total mass	State	Input
Product removal	Input or controlled	Output
Gas recycle flow rate	Input	Input

2.3.3 Kinetic Model

Common to both, the complete and reduced models, the kinetic model was based on the works of McAuley (1991), McAuley et al. (1994a, 1994b), and Zacca (1995), for Ziegler-Natta catalyst system, in which McAuley et al. (1994a) pointed out that the same kinetic model could be used for chromium-oxide catalyst systems. From this kinetic model, a simpler set of reactions was chosen (Table 2.3), resulting in the reaction rates shown in Table 2.4, and its parameters were estimated as described in the next sections.

TABLE 2.3
Set of reactions used in the models

Spontaneous site activation	$C_P \xrightarrow{k_{aSp}^k} P_0^k$
Chain initiation by monomer i	$P_0^k + M_i \xrightarrow{k_{P0i}^k} P_{\bar{\delta}_i,i}^k$
Chain propagation by monomer j	$P_{\bar{n},i}^k + M_j \xrightarrow{k_{Pij}^k} P_{\bar{n}+\bar{\delta}_j,j}^k$
Spontaneous chain transfer	$P_{\bar{n},i}^k \xrightarrow{k_{cSpi}^k} P_0^k + D_{\bar{n}}^k$
Spontaneous chain deactivation	$P_{\bar{n},i}^k \xrightarrow{k_{dSp}^k} C_d + D_{\bar{n}}^k$ $P_0^k \xrightarrow{k_{dSp}^k} C_d$

TABLE 2.4
Reaction rates

Description	Equation	Eq.
Spontaneous site activation	$R_{aSp}^k = k_{aSp}^k C_P$	(2.32)
Chain initiation by monomer i	$R_{P0i}^k = k_{P0i}^k P_0^k \left[M_{gs,i} \right]$	(2.33)
Chain propagation of end group i by monomer j	$R_{Pji}^{k,\bar{n}} = k_{Pji}^k P_{\bar{n},i}^k \left[M_{gs,j} \right]^{O_{Pji}^k}$	(2.34)
Spontaneous chain transfer of end group i	$R_{cSpi}^{k,\bar{n}} = k_{cSpi}^k P_{\bar{n},i}^k$	(2.35)
Spontaneous chain deactivation	$R_{dSpi}^{k,\bar{n}} = k_{dSp}^k P_{\bar{n},i}^k$	(2.36)
	$R_{dSp0}^k = k_{dSp}^k P_0^k$	(2.37)
Monomer i	$R_{M_i} = -\sum_{k=1}^{ns} \left(R_{P0i}^k + \sum_{j=1}^{nm} \sum_{\bar{n}}^{\bar{\bar{\infty}}} R_{Pij}^k \right)$	(2.38)
Potential sites	$R_{Cp} = -\sum_{k=1}^{ns} R_{aSp}^k$	(2.39)
Active sites	$R_{P_0^k} = R_{aSp}^k - R_{dSp0}^k + \sum_{i=1}^{nm} \left(\sum_{\bar{n}=\bar{\delta}_i}^{\bar{\infty}} R_{cSpi}^{k,\bar{n}} - R_{P0i}^k \right)$	(2.40)

TABLE 2.4 (continued)
Reaction rates

Description	Equation	Eq.
Dead sites	$R_{C_d} = \sum_{k=1}^{ns}\left(R_{dSp0}^k + \sum_{i=1}^{nm}\sum_{\bar{n}=\bar{\delta}_i}^{\bar{\infty}} R_{dSpi}^k \right)$	(2.41)
Live polymer zeroth-order momentum	$R_{\mu_{0,i}^k} = R_{P0i}^k + \sum_{j=1}^{nm}\left(k_{Pij}^k\,\mu_{0,j}^k\left[M_{gs,i} \right]^{O_{Pij}^k} - k_{Pji}^k\,\mu_{0,i}^k\left[M_{gs,j} \right]^{O_{Pji}^k} \right) - (k_{cSpi}^k + k_{dSp}^k)\,\mu_{0,i}^k$	(2.42)
Dead polymer zeroth-order momentum	$R_{\upsilon_0^k} = \sum_{i=1}^{nm}(k_{cSpi}^k + k_{dSp}^k)\,\mu_{0,i}^k$	(2.43)
Bulk polymer zeroth-order momentum	$R_{\lambda_{0,i}^k} = R_{P0i}^k$	(2.44)
Live polymer first-order momentum	$R_{\mu_{\delta_l}^k} = \sum_{i=1}^{nm}\left[\begin{array}{l} \sum_{j=1}^{nm}\left(k_{Pij}^k\left(\mu_{\delta_l,j}^k + \delta(i-l)\mu_{0,j}^k \right)\left[M_{gs,i} \right]^{O_{Pij}^k} - k_{Pji}^k\,\mu_{\delta_l,i}^k\left[M_{gs,j} \right]^{O_{Pji}^k} \right) + \\ \delta(i-l)R_{P0i}^k - (k_{cSpi}^k + k_{dSp}^k)\,\mu_{\delta_l,i}^k \end{array} \right]$	(2.45)
Dead polymer first-order momentum	$R_{\upsilon_{\delta_p}^k} = \sum_{i=1}^{nm}(k_{cSpi}^k + k_{dSp}^k)\,\mu_{\delta_p,i}^k$	(2.46)
Bulk polymer first-order momentum	$R_{\lambda_{\delta_l}^k} = \sum_{i=1}^{nm}\left(\delta(i-l)R_{P0i}^k + \delta(i-l)\sum_{j=1}^{nm} k_{Pij}^k\,\mu_{0,j}^k\left[M_{gs,i} \right]^{O_{Pij}^k} \right)$	(2.47)
Bulk polymer second-order momentum	$R_{\lambda_2} = \sum_{k=1}^{ns}\sum_{l=1}^{nm}\sum_{p=1}^{nm}\sum_{i=1}^{nm}\left[\begin{array}{l} R_{P0i}^k\,\delta(i-l)\delta(i-p) + \\ \sum_{j=1}^{nm}\left(k_{Pij}^k\left[M_{gs,i} \right]^{O_{Pij}^k}\left(\delta(i-l)\mu_{\delta_l,j}^k + \delta(i-p)\mu_{\delta_p,j}^k + \delta(i-l)\delta(i-p)\mu_{0,j}^k \right) \right) \end{array} \right]$	(2.48)

The first reaction of the set was used to represent an induction time delay seen in the chromium catalyst, besides the fact that the catalyst enters the reactor in the activated form. The chain initiation by monomer represents the first binding of an active site and a monomer. The chain propagation by monomer is responsible for growing the polymer chains (also known as live polymer chains). The spontaneous chain transfer reactions are responsible by the termination of a live polymer chain and the availability of the active site to growth a new polymer chain. The last reaction of the set is the site deactivation reaction, which turns active sites and growing polymer chains in dead sites and dead polymer chains, respectively.

2.3.4 Comparing Complete and Reduced Models

The models were implemented as S-functions (System-functions), written in C language for speed gain, to be used with the SIMULINK® (The Math Works, Inc., Natick, Massachusetts) toolbox of the software MATLAB® (The Math Works, Inc., Natick, Massachusetts). The integrator used was the ODE23s (Ordinary Differential Equation 23 stiff based on a modified Rosenbrock method) with a relative error tolerance set to 10^{-3}.

Once both models were implemented, the complete model could be used as a plant. Then, starting from a basic operating condition, some disturbances were made, as shown in Table 2.5, and some inputs and outputs from the complete model were used as inputs for the reduced model, according to Table 2.6. The outputs of both models were compared as shown in Figure 2.4 for the production and in Figure 2.5 for weight average molecular weight.

TABLE 2.5
Disturbances applied to the simulation.

Step	Time	Intensity
Mass flow of catalyst	10 hours	+50%
Bed temperature set point	50 hours	+1%
Ethylene conc. set point	150 hours	+5%

It can be observed from the results shown in Figures 2.4 and 2.5, that the reduced model dynamic responses follow the behavior of the complete model. Then, the reduced model can be used with real plant data to estimate some kinetic parameters. The bias was caused by using the concentration of the gas in the disengagement zone as input to the reduced model, instead of the concentration of the gas at the emulsion phase. A similar situation will occur when using the real plant data, because the chromatographs are also located in the disengagement zone.

2.3.5 Parameter Estimation

The relevant parameters for estimation were determined by applying a sensitivity analysis (Mahecha-Botero et al. 2009, Dehnavi et al. 2010, Rokkam et al. 2010) of all available kinetic parameters.
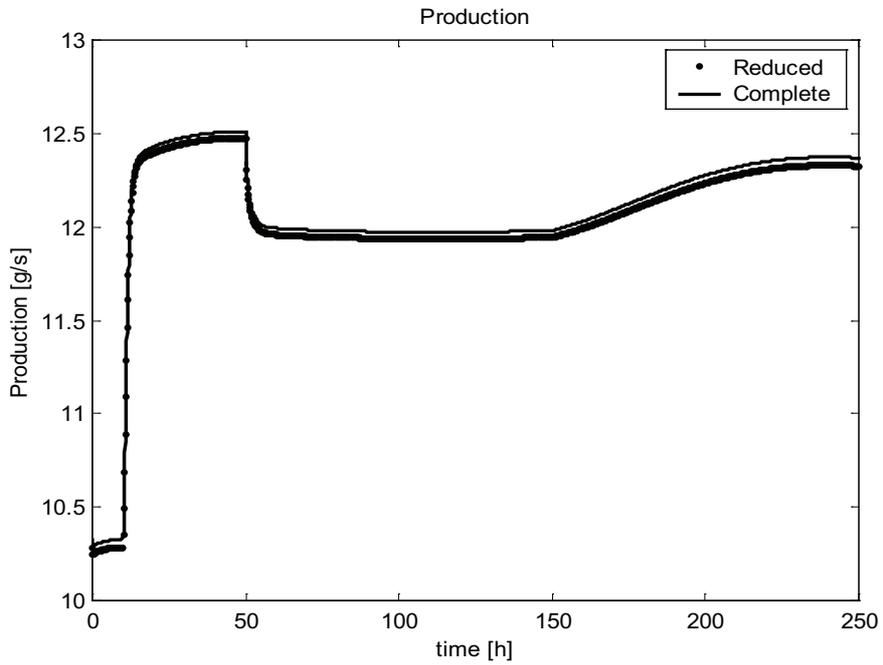
FIGURE 2.4 Production obtained as results from the complete and reduced models.
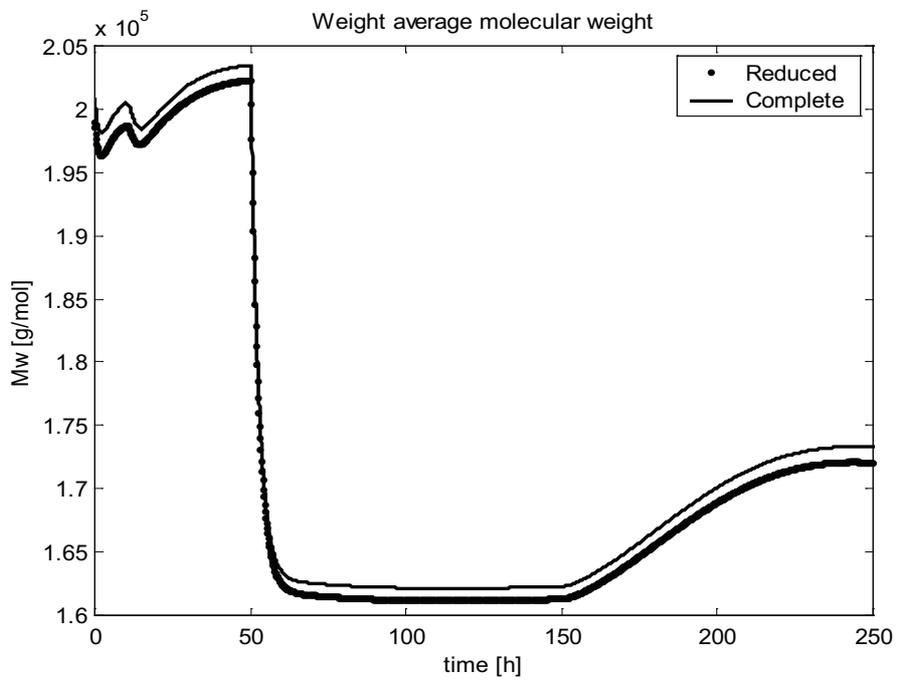
FIGURE 2.5 Weight average molecular weight obtained as results from the complete and reduced models.

The sensitivity matrix of the kinetics parameters to the outputs (W_0), generically defined in Equation 2.49, is presented in Table 2.6.

$$W_0 = -\frac{\partial y}{\partial x}\left(\frac{\partial F}{\partial x}\right)^{-1}\frac{\partial F}{\partial p} + \frac{\partial y}{\partial p} \tag{2.49}$$

In Equation 2.49, y is the system output vector and F represents the process model. The singular value decomposition of W_0 gives the most important influences of the model parameters over the outputs, which can be grouped in three different subsets (Table 2.7).

TABLE 2.6
Sensitivity matrix of the kinetics parameters to the outputs (W_0)

	K^1_{aSp}	K^1_{P01}	K^1_{P02}	K^1_{P11}	K^1_{P12}	K^1_{P21}	K^1_{P22}	K^1_{cSp1}	K^1_{cSp2}	K^1_{dSp}
Production	0.488542	2.05E-05	-5.7E-06	0.504169	0.0143	-0.00368	1.22E-05	-2.9E-05	0.000219	-0.35082
Polydispersity	-0.00031	-0.00032	0.000322	0.001332	0.000186	-0.00049	-2.2E-07	-0.00049	-0.00014	0.000224
$\bar{M}_n$	6.65E-05	0.000195	-0.0002	0.604791	0.238941	-0.23123	1.4E-05	-0.37059	-0.23887	-0.00208
$\bar{M}_w$	-0.00013	-3.4E-06	3.44E-06	0.605604	0.239052	-0.23153	1.39E-05	-0.37089	-0.23895	-0.00194
Density	1.94E-06	9.74E-06	-9.7E-06	0.002446	-0.00359	-0.0081	-1.9E-05	0.005601	0.003607	2.93E-05
Melt index-MI	0.00382	0.000102	-0.0001	-18.0324	-7.118	6.894016	-0.00041	11.04362	7.115	0.05781
	E^1_{aSp}	E^1_{P01}	E^1_{P02}	E^1_{P11}	E^1_{P12}	E^1_{P21}	E^1_{P22}	E^1_{cSp1}	E^1_{cSp2}	E^1_{dSp}
Production	-24.8371	-0.00017	4.84E-05	0.000691	1.96E-05	-5E-06	1.67E-08	0.000436	-0.00332	22.70634
Polydispersity	0.016012	0.002727	-0.00273	1.83E-06	2.55E-07	-6.8E-07	-3.1E-10	0.007463	0.002078	-0.01447
$\bar{M}_n$	-0.00338	-0.00166	0.001657	0.000829	0.000328	-0.00032	1.92E-08	5.619139	3.621894	0.134609
$\bar{M}_w$	0.006522	2.92E-05	-2.9E-05	0.00083	0.000328	-0.00032	1.91E-08	5.62366	3.623118	0.125659
Density	-9.9E-05	-8.3E-05	8.26E-05	3.35E-06	-4.9E-06	-1.1E-05	-2.7E-08	-0.08493	-0.0547	-0.0019
Melt index-MI	-0.19421	-0.00087	0.000868	-0.02472	-0.00976	0.00945	-5.7E-07	-167.449	-107.882	-3.74162

TABLE 2.7
Groups formed by de singular values decomposition of the matrix W_0

Group	Output	Parameters
1	Melt Index - MI	$K_{P11}^1, K_{P12}^1, K_{P21}^1, K_{cSp1}^1, K_{cSp2}^1, E_{cSp1}^1, E_{cSp2}^1$ and E_{dSp}^1
2	Production	$K_{aSp}^1, K_{P11}^1, K_{dSp}^1, E_{aSp}^1, E_{cSp1}^1$ and E_{dSp}^1
3	Density	$K_{P11}^1, K_{P21}^1, E_{cSp1}^1$ and E_{cSp2}^1

It is possible to observe that the parameters grouped under each output are in agreement with the expected results, and that all outputs must be estimated together, as the groups are connected by some common parameters. The procedure of sensitivity analysis should be repeated after each step of the estimation as it could be changing with the parameters during the estimation.

The estimation procedure was done in two steps: one using experimental data of homopolymer production, and other using copolymer production, keeping constant the parameters responsible for the gross production rate. A maximum likelihood estimation method was applied to estimate the parameters, using the Nelder-Mead minimization method (Nelder and Mead 1965). The activation energies of the same reaction with different monomers were set equal, as well as the pre-exponential factor of the initiation by monomer reactions.

The estimated parameters are presented in Table 2.8 as reaction constants calculated at a temperature of 100^oC. The correlation matrix obtained from the estimated parameters is presented in Table 2.9, in which it should be noted, as expected, that the pre-exponential factors had strong correlation with its respective activation energy.

The valor of parameters presented in Table 2.8 cannot be compared to others found in the literature, because the literature works are based on Ziegler-Natta catalyst system, and the present work deals with a chromium-oxide catalyst system.

2.3.6 Tests in Pilot Plant

The results obtained with both models are shown in Figures 2.6 and 2.7, in which 70 hours of experimental data from a pilot plant have been used in the simulations, being the first 50 hours of the experimental data used in the estimation procedures (with other datasets) and the last 20 hours reserved to validate the models. Catalyst pulses were performed (Figure 2.8) at different temperature levels (Figure 2.9), allowing enough time between the pulses for the active catalyst inventory to decay.

TABLE 2.8
Reaction constants calculated at 100°C

Reaction	Reaction constant
Spontaneous site activation	9.58×10^{-6} s^{-1}
Chain initiation by ethylene	4.28×10^{6} cm^{3}/(mol.s)
Chain initiation by butene	4.28×10^{6} cm^{3}/(mol.s)
Chain propagation of end group ethylene by ethylene	2.92×10^{5} cm^{3}/(mol.s)
Chain propagation of end group butene by ethylene	1.13×10^{4} cm^{3}/(mol.s)
Chain propagation of end group ethylene by butene	1.44×10^{5} cm^{3}/(mol.s)
Chain propagation of end group butene by butene	7.84×10^{2} cm^{3}/(mol.s)
Spontaneous chain transfer from end group ethylene	4.68×10^{-2} s^{-1}
Spontaneous chain transfer from end group butene	2.91×10^{-2} s^{-1}
Spontaneous chain deactivation	1.93×10^{-2} s^{-1}

TABLE 2.9
Correlation matrix of some estimated kinetics parameters

	K_{P11}^1	K_{aSp}^1	E_{aSp}^1	K_{dSp}^1	E_{dSp}^1	K_{cSp1}^1	E_{cSp1}^1
K_{P11}^1	1	-0.435	0.383	0.074	0.079	0.180	-0.197
K_{aSp}^1	-0.435	1	0.608	-0.004	0.021	-0.199	-0.035
E_{aSp}^1	0.383	0.608	1	-0.009	0.034	-0.063	-0.210
K_{dSp}^1	0.074	-0.004	-0.009	1	0.915	-0.293	-0.325
E_{dSp}^1	0.079	0.021	0.034	0.915	1	-0.324	-0.364
K_{cSp1}^1	0.180	-0.199	-0.063	-0.293	-0.324	1	0.927
E_{cSp1}^1	-0.197	-0.035	-0.210	-0.325	-0.364	0.927	1
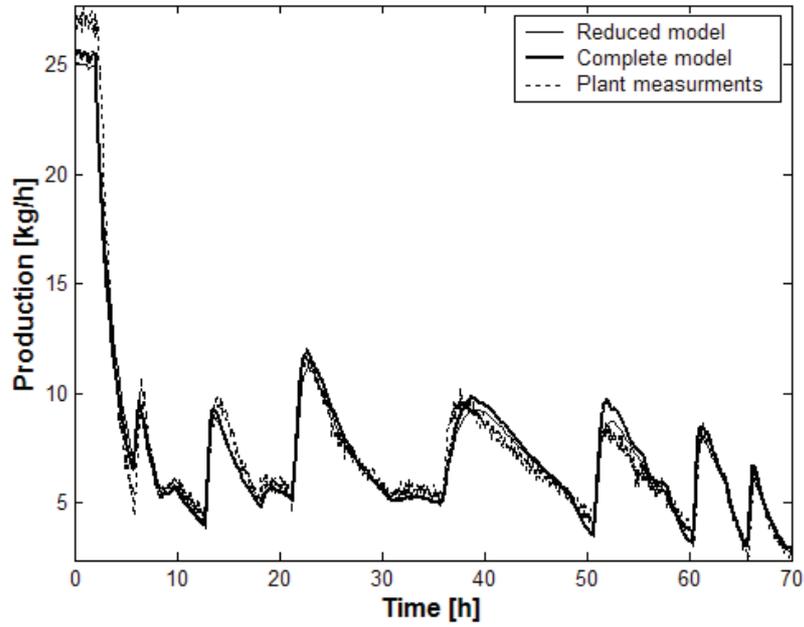
FIGURE 2.6 The plant measured production and the model simulated productions.
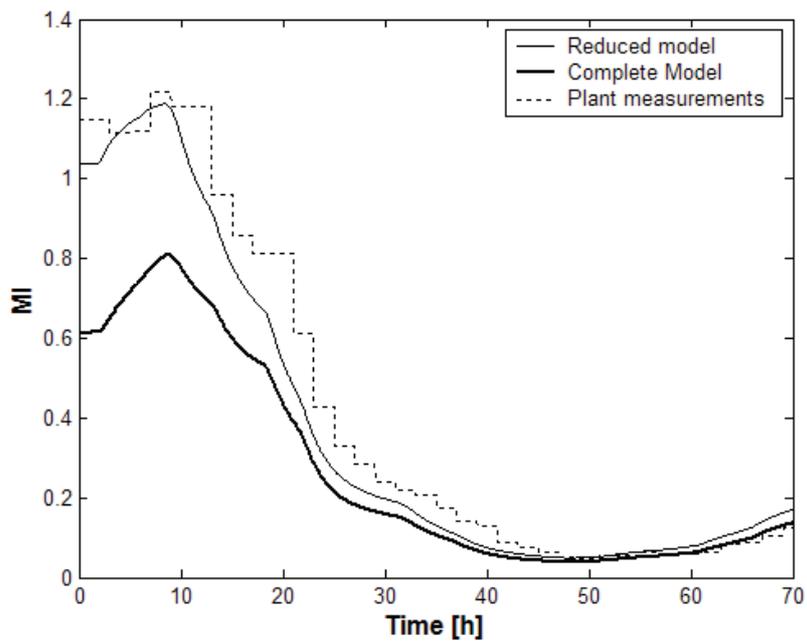
FIGURE 2.7 The plant measured melt index (MI) and the model simulated melt indexes.
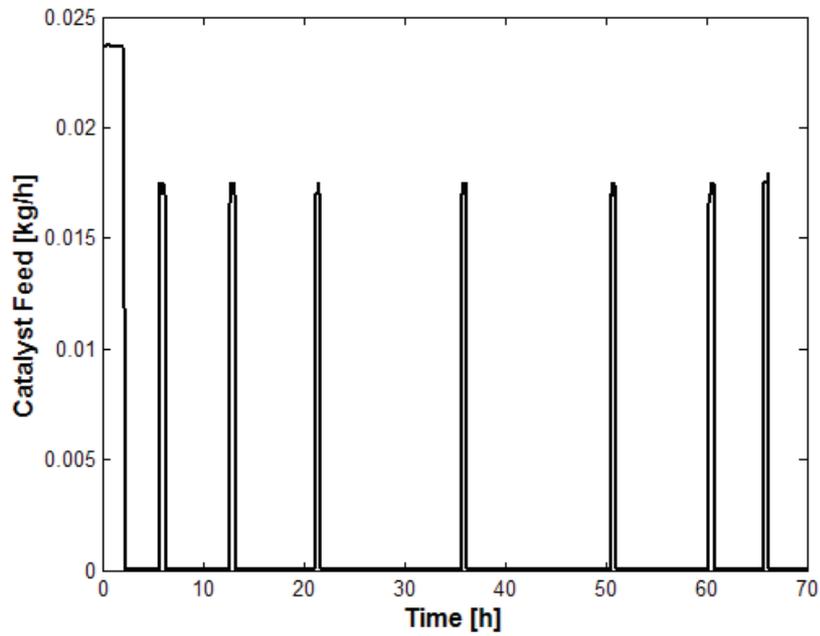
FIGURE 2.8 Catalyst feed pulses applied to the plant.
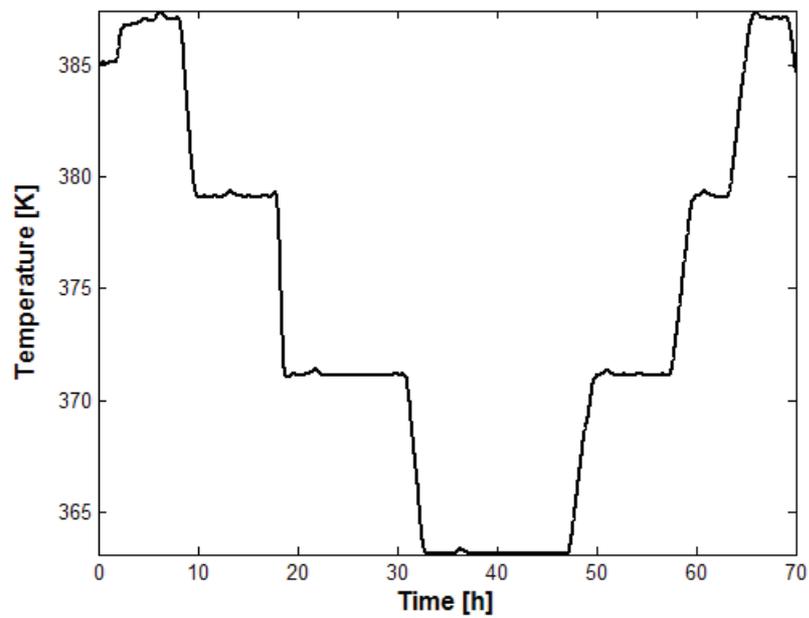
FIGURE 2.9 Plant measured fluidized-bed temperature, showing the temperature levels used in the experiments.

It can be observed in Figure 2.6, the good agreement between the plant data and the predictions of the models for polymer production. The small bias between the complete and reduced models can also be observed in this result, as one presented in Figure 2.4.

In Figure 2.7, the larger difference between the complete model and the plant data for the first 15 hours may be associated to the initial condition for the models, assumed to be at the steady state. Other datasets used in the estimation and validation of the models were presented in Gambetta (2001), showing similar behaviors.

The main relevance of this work is the methodology that takes a complete model, developed for use in control and process studies, replaces some of its states by their correspondent plant measurements, resulting in a reduced model that is easier to use in the parameter estimation stage. As shown in the results, the application of this methodology does not imply in any significant loss of information, in terms of production and properties. The reduced model allows faster and easier parameter estimation when compared to the complete model.

2.3.7 Simplified Models

Many published studies on polymerization modeling have been focused on parameter estimation and industrial applications of both, phenomenological and empirical models, to design nonlinear model predictive controllers (Zhao et al. 2001, Soroush 1998). In the work of Neumann et al. (2006), the complete phenomenological model, described in this Section, and a set of empirical models built based on industrial data and nonlinear Partial Least Squares (PLS) were compared with respect to the capability of predicting the MI and polymer yield rate of a low density polyethylene production process constituted by two FBRs connected in series.

The empirical models are based on three versions of the PLS regression approach, differing from each other in the mapping function used to determinate the subspace where the regression is performed. The linear PLS (Wold 1996) uses the mapping function $\hat{\mathbf{y}} = b\,\mathbf{t}$, the Quadratic PLS (QPLS) (Baffi et al. 1999) uses the polynomial mapping function $\hat{\mathbf{y}} = b_0 + b_1\,\mathbf{t} + b_2\,\mathbf{t}^2$, and the Box-Tidwell PLS (BTPLS) (Li et al. 2001) uses a highly flexible nonlinear mapping function: $\hat{\mathbf{y}} = b_0 + b_1\,\text{sign}(\mathbf{t})^\delta\,|\mathbf{t}|^\alpha$. Among the tested empirical models, the QPLS model is more appropriate to describe the polymer yield rate and MI behavior and also presented better results than the phenomenological model for closed-loop control application (Neumann et al. 2006).

In a studied industrial application example, Neumann et al. (2006) showed that the empirical model was suitable as a virtual analyzer for polymer properties and the phenomenological model was important to design a Nonlinear Model Predictive Controller (NMPC) for the MI. This approach has improved the controller action and the polymer quality by reducing significantly the process variability, showing that the combination of these two types of models can be a good alternative to advanced process control.

2.4 Control of Gas-Phase Polymerization Reactors

Production and quality control and stabilization of gas-phase polymerization reactors are challenging problems and need to be addressed through good control strategies. Dadedo et al. (1997) and Salau et al. (2008, 2009) have demonstrated based on phenomenological models that, without feedback control, industrial gas-phase polyethylene reactors are prone to unstable steady states, limit cycles, and excursions toward unacceptable high-temperature steady states. In their work, the ability of the controllers to stabilize desired set-points of industrial interest was evaluated using a bifurcation approach.

2.4.1 Temperature Control

Despite in the literature (Dadedo et al. 1997, Ghasen 2000, McAuley et al. 1995), the nonlinear dynamic behaviors found in gas-phase polymerization reactors have been modeled through modifications in the kinetic parameters of reactor models, in the work of Salau et al. (2008), the kinetic parameters have been fitted to industrial plant data, as shown in the previous section, and the obtained model is able to predict and explain several dynamic behaviors found in a real unit, as shown in Figures 2.10 and 2.11. The Hopf bifurcation behavior was achieved as a consequence of loosing the temperature control as a result of control valve saturation at high production throughput (Salau 2004).
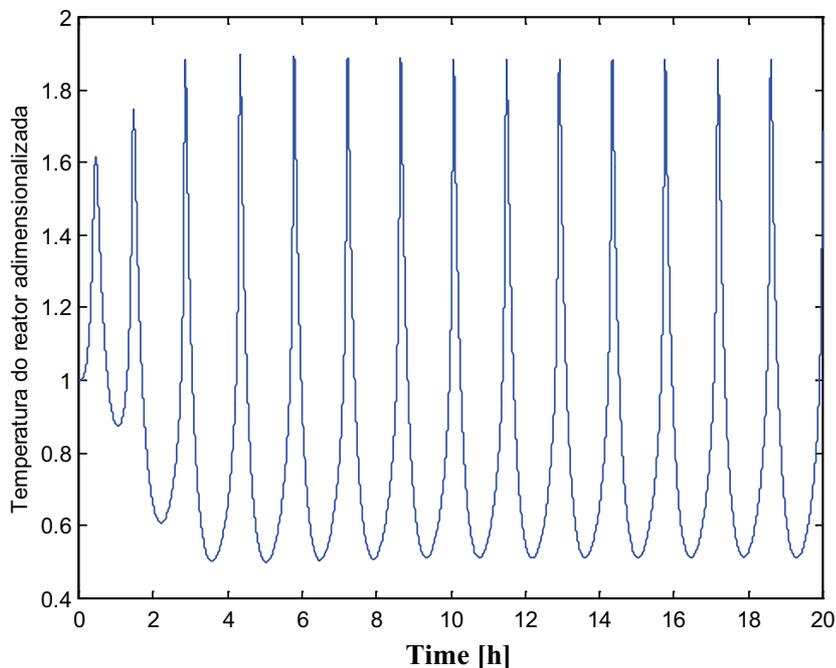
FIGURE 2.10 Limit cycle obtained with the reactor temperature in open loop after disturbing the catalyst feed rate.
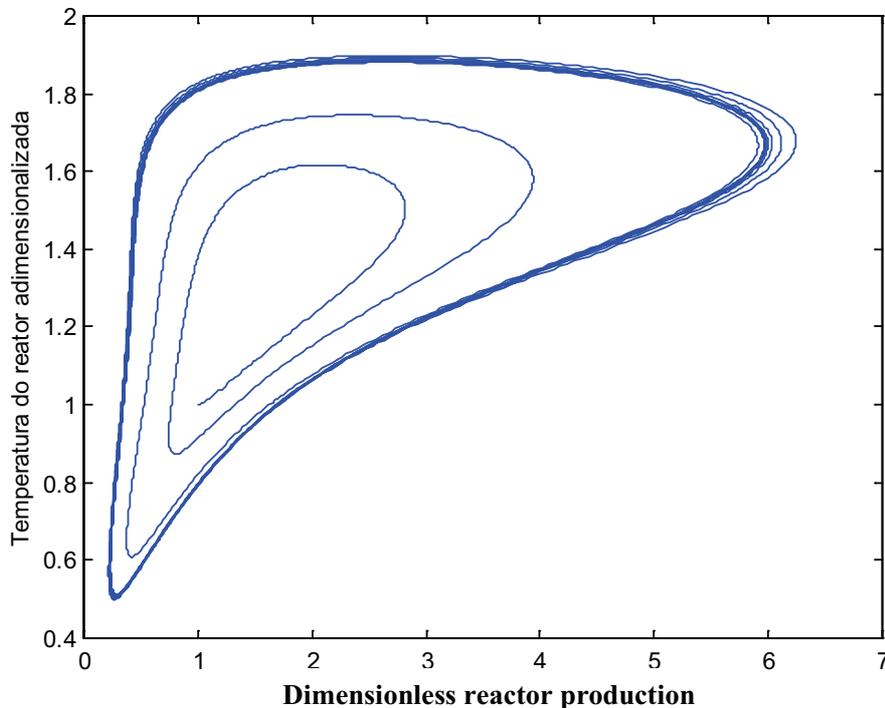
FIGURE 2.11 Limit cycle in the reactor temperature and production state subspace obtained after disturbing the catalyst feed rate.

The unstable steady states and limit cycles can be explained mathematically by the presence of Hopf bifurcation points, where complex conjugate pairs of eigenvalues of the Jacobian matrix of the dynamic model cross the imaginary axis (Doedel et al. 2002). Physically, the oscillatory behavior can be explained by positive feedback between the reactor temperature and the reaction rate (McAuley et al. 1995). If the reactor temperature is higher than the unstable steady-state temperature, then the heat removal in the heat exchanger, Figure 2.1, is above the steady-state heat-generation rate. As a result, the reactor temperature starts to decrease, decreasing the reaction rate. Thus, catalyst and monomer begin to accumulate in the reactor, increasing the temperature, the rate of reaction, and the product outflow rate, resuming the limit cycle (Salau et al. 2008).

When there is no saturation in the cooling water control valve, tight regulation of the bed temperature with a simple Proportional-Integral-Derivative (PID) controller is enough to ensure reactor stability (Dadedo et al. 1997, Salau et al. 2008, Seki et al. 2001). However, system thermal limitation, which bottlenecks the heat exchanger, is a common situation in the industry causing the reactor to operate without a feedback temperature controller, leading to oscillatory behavior and limit cycles. Therefore, the saturation in the manipulated variable of the reactor temperature controller should be avoided to prevent complex nonlinear dynamic behaviors.

Salau et al. (2009), using bifurcation analysis with the complete phenomenological model described in the previous section, determined a set of auxiliary manipulated variables to be used in a multivariable control strategy for the reactor temperature control that successfully removed the saturation in the manipulated variable. The candidate auxiliary manipulated variables were catalyst feed rate, inert saturated organic feed rate, and ethylene partial-pressure controller set-point. All these variables can stabilize the reactor temperature controller in the desired set-point by reducing the rate of heat generation or increasing the heat transfer capacity, but can also reduce the production rate, then must be used optimally. Results from Salau et al. (2009) suggest that the use of gain-scheduling strategy in the PID temperature controller with a Model Predictive Controller (MPC) for the auxiliary manipulated variables is a satisfactory solution to avoid the saturation of the manipulated variable and, hence, the undesired nonlinear dynamic behavior, reducing the production loss and improving the product quality.

2.4.2 Gas-Phase Composition Control

Multivariable predictive controllers are a class of control algorithms using phenomenological or empirical models of process to predict future responses of the plant, based on the modification of the manipulated variables calculated over a horizon of control. Thus, the MPC generates control actions, in general set-points, for the regulatory control layer of the plant, by solving an optimization problem in real time, where error is minimized over a prediction horizon, subject to constraints on manipulated and controlled variables. This ability of MPC controllers to deal with constraints that vary over time allows the controller to drive the plant to optimal economic conditions.

The main controlled variables for control composition of gas phase FBRs are concentration of ethylene, hydrogen/ethylene ratio and co-monomer/ethylene ratio. The concentration of ethylene in the gas phase is used to control the rate of polymer production because it is directly linked to the rate of propagation of the polymer chain. The ethylene flow rate is the manipulated variable in this case. All other feed gas flow, gas temperature, total gas phase pressure, level of the fluidized-bed, among others, are considered disturbances. For some operational reasons, such as maximum rate of discharge of product from the reactor, the maximum concentration of ethylene is treated generally as a constraint. The control of the ratio hydrogen/ethylene (H_2/C_2) is important to maintain the polymer viscosity in the FBR, measured by the MI. Control of H_2/C_2 is, in general, done through cascade control, which is assigned as set-point for the relationship H_2/C_2, which is the master loop that sends the set-point to the hydrogen flow control loop of the FBR, both consisting of PID controllers. Moreover, for many products, the relationship H_2/C_2 should be controlled through the purge flow of the monomer recovery system in order to de-concentrate the whole hydrogen system. In the MPC controller, the manipulated variables for the H_2/C_2 relationship are the injecting hydrogen and the light gas purge. The flow rates of catalyst, ethylene and co-monomer are disturbances for this relationship, because they affect the reactivity of the mixture and change the concentration of ethylene. Likewise, less influential, temperature, pressure and level of the bed are considered as disturbances.

The control of co-monomer/ethylene ratio is important to regulate the mechanical properties of each resin of polymer. Similar to H_2/C_2, the relationship co-monomer/ethylene ratio is

controlled by the feed flow rate of co-monomer. The ethylene flow rate is treated as disturbance for this relationship.

2.4.3 Production Control

Control of production rate usually is associated with the optimization of production in the reactor, or the relationship between production rates of reactors in series. In this case, a NMPC is used as part of the control strategy, transferring set-points for the control of composition, which may be the same NMPC or a set of slave PIDs. The controller-optimizer receives the production goals of the operator and calculates the control actions of the manipulated variables, which are the flow rates of catalyst and monomer, under the constraints of pressure and catalytic yield, especially when the process involves more than one reactor in series. The operating conditions that directly affect the residence time and polymerization rate, as the level of the bed, the reactor temperature and feed flow rates of the other components, are considered disturbances.

2.4.4 Quality Control

Most of the mechanical properties of the polymer formed in FBRs are related to the MI and density. The control of these two properties will ensure that the product is within specifications. For chromium-oxide catalyst systems, the control of MI is done via manipulation of the reactor temperature. For Ziegler-Natta catalyst systems, the control of MI is through H_2/C_2 manipulation in the gas phase. The density control is done by manipulating the co-monomer/ethylene ratio.

Virtual analyzers are used to predict these properties because they measurements come from laboratory analysis with a high sampling time. Thus, the controllers can calculate the control actions faster than the laboratory sampling time, and each new laboratory analysis is used in the correction mechanism of the virtual analyzer. The other variables that have a direct influence on MI and density are considered disturbances.

2.4.5 Industrial Application of Non-linear Model Predictive Control

To illustrate the applicability of the developed models, an empirical model for the MI was used as virtual analyzer and the phenomenological model (Neumann et al. 2006), as described in the previous Section, was used to design a NMPC to maintain the MI at the set-point and to reduce the off-specification products. The NMPC uses linear dynamics and nonlinear gains obtained from the phenomenological model. The virtual analyzer was implemented with a first-order filtered ratio factor in each analysis of the laboratory (around each 2 hours) to update the parameters of the empirical model and to account for the time lag required for laboratory measurements. The NMPC manipulated variable is the ratio between hydrogen and ethylene gas-phase mole fraction.

Figure 2.12 shows historical data of MI when in opened loop (a) and closed loop (b). The MI data correspond to measurements performed in laboratory from samples taken at each two hours. The virtual analyzer used in the closed loop provides predicted values of MI to the controller at time intervals of one minute, improving the controller action and the polymer quality, as observed in Figure 2.12b where the dashed line at normalized MI = 1 is the set-point. As can be observed in Figure 2.13, which shows the distribution curves of the polymer MI for opened and closed loop data, the variability was significantly reduced by the controller. It is important to observe that the dashed lines at normalized MI equal to 0.8 and 1.2 in Figures 2.12 and 2.13 correspond to the lower and upper MI specification limits.

(a)   (b)
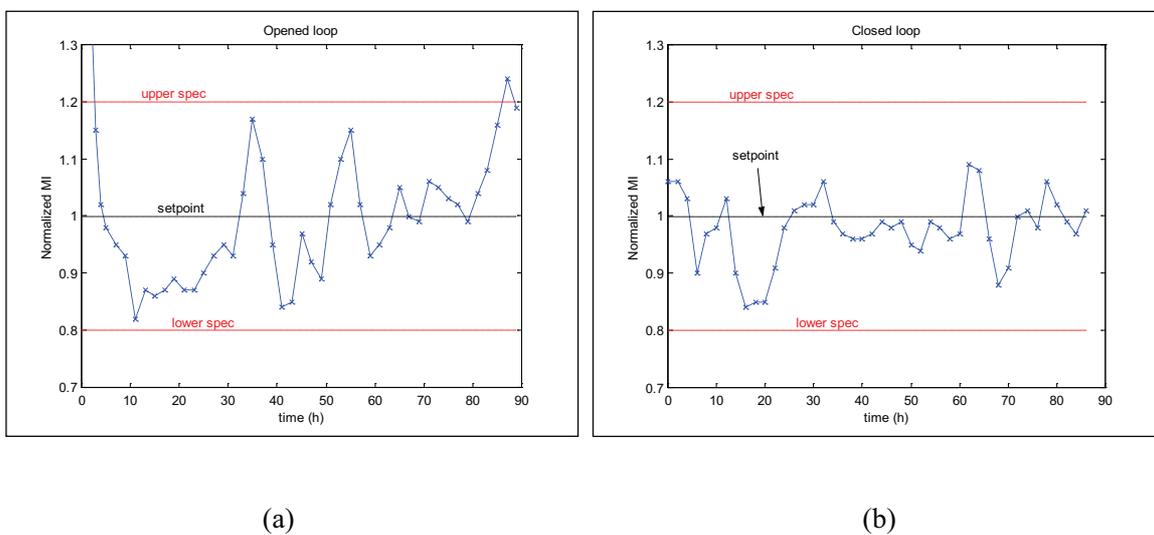
FIGURE 2.12 Historical data of melt point (MI) when in opened loop (a) and closed loop (b).

Consequently, data presented in Figures 2.12 and 2.13 indicate that the closed loop strategy reduced the off-specification products. These results are confirmed by evaluating the process capability index (C_{PK}), defined as the ratio between permissible deviation, measured from the mean value to the nearest specific limit of acceptability and the actual one-sided 3σ spread of the process, and taking into account that larger values of C_{PK} mean higher product quality. The C_{PK} for the opened loop was 0.40 ($\sigma = 0.15$) and for the closed loop was 1.00 ($\sigma = 0.06$). The NMPC improved the polymer quality by reducing significantly the process variability (Neumann et al. 2006).
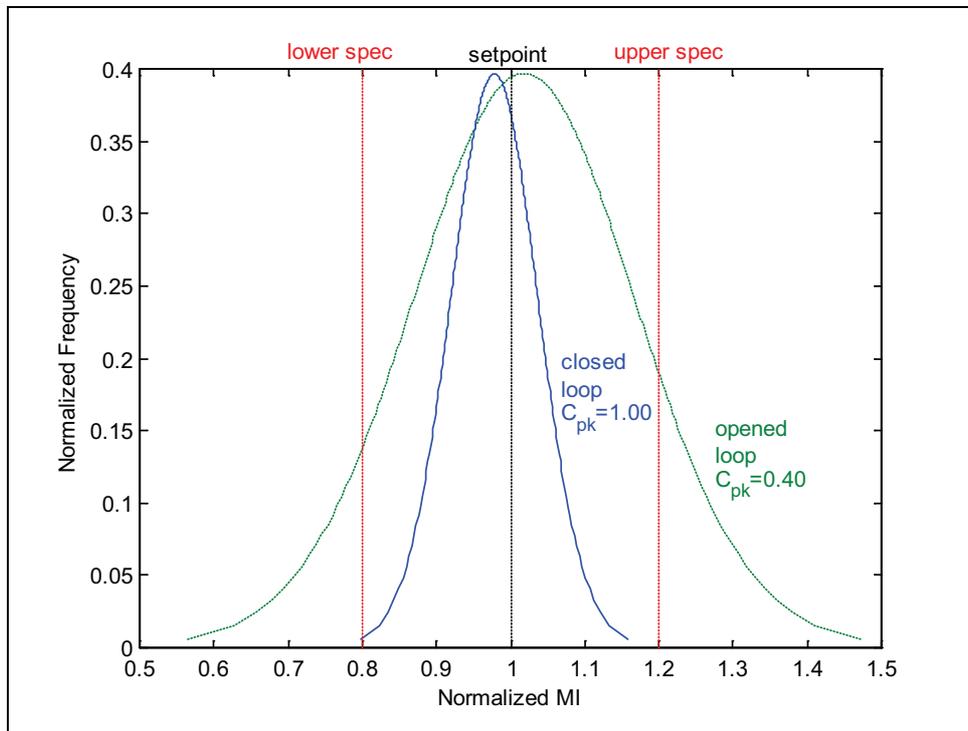
FIGURE 2.13 Distribution curves for the opened loop and the closed loop.

2.5 Conclusions

The present work has shown that the model structure traditionally applied to the process simulation of gas-phase polymerization reactors can be modified to attain better and faster parameter estimation. This has been done by considering some of the states present in a rigorous process model (or complete model for short) as inputs of a corresponding reduced model when the respective plant measured variables are available. The structure of the complete model needs a number of controllers to stabilize the system, whose tuning parameters depend on the estimated kinetic parameters. The reduced model has been proposed to remove the interaction between the control loop parameters and the kinetic parameters to be estimated, taking advantage of plant measurements not used directly by the previous model. The experimental data have been obtained from a UNIPOL pilot plant using a chromium-oxide catalyst system producing polyethylene and copolymer with butene. The reduced model allows faster and easier parameter estimation when compared to the complete model.

The process control applications have shown that an empirical model is more appropriate as a virtual analyzer for polymer properties than the phenomenological model, being this later used to

design a nonlinear model predictive controller for the MI. This combined use of empirical and phenomenological models has improved the controller action and the polymer quality by reducing significantly the process variability, showing that this approach can be a good alternative to advanced process control.

Specific Nomenclature

A	reactor area at the fluidized bed region
c_{p0}	specific heat of the gas phase entering the fluidized bed
c_{pb}	specific heat of the bubble phase
c_{pg}	specific heat of the gas phase
c_{ps}	specific heat of the solid phase
c_{Tb}	total concentration of the bubble phase
C_d	dead site
C_D	drag coefficient
C_P	potential site
d_b	effective bubble diameter
d_{bm}	maximum bubble diameter
d_{bo}	initial bubble diameter
d_p	particle diameter
$D_{\bar{n}}^{k}$	dead polymer with $\bar{n}$ monomers of site k
D_g	gas diffusivity coefficient
E_i^j	activation energy of the reaction i at the site j, in which i may be aSp, $P0$, P, cSp and dSp, denoting respectively, spontaneous activation, initiation by monomer, propagation, spontaneous chain transfer and spontaneous deactivation
$[\bar{E}_{i,b}]$	mean concentration of component i in the bubble phase
$[E_{i,b}^{k}]$	concentration of component i of the gas going out from the bubble phase at the bed top
$[E_{i,g}]$	concentration of component i in the gas phase
$[E_{i,0}]$	concentration of component i in the gas entering the bed from below
$[E_{d,i}]$	concentration of the component i in the disengagement zone
f_c	crystallinity factor
$F_{E_i,f}$	molar flux of component i feed in the fluidized bed
g	gravity acceleration

H height of the fluidized bed

H_{bc} heat transfer between bubble and cloud-wake region

H_{be} heat transfer coefficient between the bubble and gas phases

H_{be} heat transfer between bubble and emulsion phases

H_{ce} heat transfer between cloud-wake region and emulsion phase

K_i^j pre-exponential factor of the reaction i at the site j, in which i may be *aSp*, *P0*, *P*, *cSp* and *dSp*, denoting respectively, spontaneous activation, initiation by monomer, propagation, spontaneous chain transfer and spontaneous deactivation

K_{bc} mass transfer between bubble and cloud-wake region

K_{be} mass transfer coefficient between the bubble and gas phases

K_{be} mass transfer between bubble and emulsion phases

K_{ce} mass transfer between cloud-wake region and emulsion phase

m_g mass of gas in the emulsion phase

m_s mass of solids in the emulsion phase

M_i monomer of type i

$\overline{M}_b$ mean molecular weight of the gas in the bubble phase

$\overline{M}_{M,i}$ molecular mass of the monomer i

$\overline{M}_i$ molecular mass of the component i

$\overline{M}_n$ number average molecular weight

$\overline{M}_w$ mass average molecular weight

nc number of components

nm number of monomers

P_0^k active site of type k

$P_{\bar{\delta},i}^k$ initiated chain with monomer type i and site type k

$P_{\bar{n},i}^k$ live polymer with $\bar{n}$ monomers, with end group i and active site k

Q_p volumetric flow of product

Q_v vent volumetric flow

$R_{E,i}$ reaction rate

T temperature of the gas phase

$\overline{T}_b$ mean temperature of the bubble phase

T_b^h temperature of the gas going out from the bubble phase at the bed top

T_d disengagement zone temperature

T_0 temperature of the gas entering the fluidized bed from bellow

U_0 gas velocity at the fluidized bed bottom

U_b gas ascending speed through the fluidized bed

U_e upward superficial velocity of gas through the emulsion phase

U_T terminal velocity

V_b bubble phase volume

V_d volume of the disengagement

W_f mass flow of solid feed to the reactor

Greek letters

δ^* bubble fraction in the fluidized bed

ΔH_{R_i} polymerization reaction heat

ε_{mf} fluidized bed porosity

μ gas viscosity

ρ_d specific mass of the gas in the disengagement zone

ρ_{g0} specific mass of the gas entering the fluidized bed from below

χ swelling factor

Dimensionless groups

Ar Archimedes number

Re_{mf} Reynolds number in minimum fluidization conditions

Re_p particle Reynolds number

REFERENCES

Alizadeh, M., Mostoufi,N., Pourmahdian, S., and Sotudeh-Gharebagh, R. 2004. Modeling of fluidized bed reactor of ethylene polymerization. *Chem. Eng. J.* 97:27-35.

Baffi, G., Martin, E.B. and Morris, A.J. 1999. Non-linear projection to latent structures revisited: The quadratic PLS algorithm. *Comput. Chem. Eng*. 23:395-411.

Chen, X.Z., Shi, D.P., Gao, X., and Luo, Z.H. 2011. A fundamental CFD study of the gas-solid flow field in fluidized bed polymerization reactors. *Powder Technol*. 205:276-288.

Chen, X.Z., Luo, Z.H., Yan, W.C., Lu, Y.H., and Ng, I.S. 2011. Three-dimensional CFD-PBM coupled model of the temperature fields in fluidized-bed polymerization reactors. *AIChE J.* 57(12): 3351-3366.

Choi, K.Y. and Ray, W.H. 1985. The dynamic behavior of fluidized bed reactors for solid catalyzed gas phase olefin polymerization. *Chem. Eng. Sci.* 40:2261-2279.

Dadedo, S.A., Bell, M.L., McLellan, P.J., and McAuley, K.B. 1997. Temperature control of industrial gas-phase polyethylene reactors. *J. Process Control* 7:83-95.

Dehnavi, M.A., Shahhosseini, S., Hashemabadi, S.H., and Ghafelebashi, M. 2010. CFD simulation of hydrodynamics and heat transfer in gas phase ethylene polymerization reactors. *Int. Commun. Heat Mass Transfer* 37:437-442.

Doedel, E.J., Paffenroth, R.C., Champneys, A.R. et al. 2002. AUTO 2000: Continuation and bifurcation software for ordinary differential equations (with HomCont). California Institute of Technology: Pasadena, CA. http://www.dam.brown.edu/people/sandsted/ publications/auto2000.pdf (accessed October 26, 2012).

Embiruçu, M., Lima, E.L., and Pinto, J.C. 1996. A survey of advanced control of polymerization reactors. *Polym. Eng. Sci.* 36:433-447.

Fernandez, F.A.N., and Lona, L.M.F. 2001. Heterogeneous modeling for fluidized-bed polymerization reactor. *Chem. Eng. Sci.* 56:963-969.

Fernandez, F.A.N., Lona, and L.M.F. 2004. Multizone circulating reactor modeling for gas-phase polymerization: I. Reactor modeling. *J. Appl. Polym Sci.* 93(3): 1042-1052.

Gambetta, R. 2001. Modeling and simulation of fluidized bed polymerization reactors (Modelagem e simulação de reatores de polimerização em leito fluidizado). M.Sc. diss. Federal Univ. of Rio Grande do Sul (Universidade Federal do Rio Grande do Sul). (In Portuguese).

Gambetta, R., Zacca, J.J., and Secchi, A.R. 2001. Model for estimation of kinetics Parameters in gas-phase polymerization reactors. *In Proceedings of the 3rd Mercosur Congress on Process Systems Engineering* (ENPROMER 2001), CD-ROM, vol. II: 901-906, Santa Fé, Argentina.

Ghasem, N.M. 2000. Dynamic behavior of industrial gas phase fluidized bed polyethylene reactors under PI control. *Chem. Eng. Technol.* 23(2):133-140.

Ibrehema, A.S., Hussaina, M.A., and Ghasemb, N.M. 2009. Modified mathematical model for gas phase olefin polymerization in fluidized-bed catalytic reactor. *Chem. Eng. J.* 149:353–362.

Jafari, R., Sotudeh-Gharebagh, R., and Mostoufi, N. 2004. Modular simulation of fluidized bed reactors. *Chem. Eng. Technol.* 27:123–129.

Kiashemshaki, A., Mostoufi, N., Sotudeh-Gharebagh, R., and Pourmahdian, S. 2004. Reactor modeling of gas-phase polymerization of ethylene. *Chem. Eng. Technol.* 27:1227-1232.

Kiashemshaki, A., Mostoufi, N., and Sotudeh-Gharebagh. 2006. Two-phase modeling of a gas phase polyethylene fluidized bed reactor. *Chem. Eng. Technol.* 61:3997-4006.

Kunii, D. and Levenspiel, O. 1991. *Fluidization Engineering*, 2nd edn. Newton: Butterworth-Heinemann.

Lagemann, B. 1989. Modeling, simulation and control of fluidized bed reactor for the gas phase polymerization of olefins. M.Sc. diss., University of Wisconsin.

Li, B., Martin, E.B., and Morris, A.J. 2001. Box-Tidwell based partial least squares regression. *Comput. Chem. Eng*. 25:1219-1233.

Mahecha-Botero, A., Grace, J.R., Elnashaie, S.S.E.H., and Lim, C.J. 2009. Advances in modeling of fluidized-bed catalytic reactors: A comprehensive review. *Chem. Eng. Commun.*196:1375-1405.

McAuley, K.B. 1991. Modeling, estimation and control of product properties in a gas phase polyethylene reactor. Ph.D. diss., McMaster Univ.

McAuley, K.B., Xie, T., Hsu, J.C.C., and Bacon, D.W. 1994a. Gas phase ethylene polymerization: Production process, polymer properties, and reactor modeling. *Ind. Eng. Chem. Res.* 33:449-479.

McAuley, K.B., Talbot, J.P., and Harris, T.J. 1994b. A comparison of two-phase and well-mixed models for fluidized-bed polyethylene reactors. *Chem. Eng. Sci*. 49:2035-2045.

McAuley, K.B., MacDonald, D.A., and McLellan, P.J. 1995. Effects of operating conditions on stability of gas-phase polyethylene reactors. *AIChE J*. 41(4):868-879.

Meier, G.B., Weickert, G., and van Swaaij, W.P.M. 2002. FBR for catalytic propylene polymerization: Controlled mixing and reactor modeling. *AIChE J*. 48:1268-1283.

Nelder, J.A. and Mead R. 1965. A simplex method for function minimization. *Comput. J.* 7:308-313.

Neumann, G.A., Finkler, T.F., Cardozo, N.S.M., and Secchi, A.R. 2006. Comparison between phenomenological and empirical models for gas-phase polymerization process control. *Ind. Eng. Chem. Res*. 45(8):2651-2660.

Peacock, A.J. 2000. *Handbook of Polyethylene*. Basel-New York: Marcel Dekker, Inc.

Ray, W.H. 1997. POLYRED Users's Manual Version 4.1. University of Wisconsin. http://polyred.che.wisc.edu (accessed October 26, 2012).

Reginato, A.S. 2001. Modeling and simulation of liquid-phase polimerization reactors of SHERIPOL process (Modelagem e Simulação dos Reatores de Polimerização em Fase Líquida do Processo SPHERIPOL). M.Sc. diss., Federal Univ. of Rio Grande do Sul (Universidade Federal do Rio Grande do Sul). (In Portuguese).

Rokkam, R.G., Fox, R.O., and Muhle, M.E. 2010. Computational fluid dynamics and electrostatic modeling of polymerization fluidized-bed reactors. *Powder Technol.* 203:109-124.

Salau, N.P.G. 2004. Control of temperature in gas-phase polymerization reactors (Controle de temperatura em reatores de polimerização em fase gasosa). M.Sc. diss., Federal Univ. of Rio Grande do Sul (Universidade Federal do Rio Grande do Sul). (In Portuguese).

Salau, N.P.G., Neumann, G.A., Trierweiler, J.O., and Secchi, A.R. 2008. Dynamic behavior and control in an industrial fluidized-bed polymerization reactor. *Ind. Eng. Chem. Res.* 47:6058-6069.

Salau, N.P.G., Neumann, G.A., Trierweiler, J.O., and Secchi, A.R. 2009. Multivariable control strategy based on bifurcation analysis of an industrial gas-phase polymerization reactor. *J. Process Control* 19:530-538.

Secchi, A.R., Santos, M.G., Neumann, G.A., and Trierweiler, J.O. 2001. A dynamic model for a FCC UOP stacked converter unit. *Comput. Chem. Eng*. 25:851–858.

Seki, H., Ogawa, M., and Oshima, M. 2001. PID temperature control of an unstable gas-phase polyolefin reactor. *J. Chem. Eng. Jpn*. 42:1415-1422.

Soroush, M. 1998. State and parameter estimations and their applications in process control. *Comput. Chem. Eng*. 23:229-245.

Wold, H. 1966. Nonlinear estimation by iterative least squares procedures. *In Research Papers in Statistics*, ed. F. David*, 411-444. New York: Wiley.

Zacca, J.J. 1995. Distributed parameter modeling of the polymerization of olefins in chemical reactors. PhD diss., Univ. of Wisconsin.

Zhao, H., Guiver, J., Neelakantan, R., Biegler, L.T. 2001. A nonlinear industrial model predictive controller using integrated PLS and neural net state-space model. *Control Eng. Pract*. 9(2):125-133.